CF, CF_2 and SiF densities in inductively driven discharges containing C_2F_6, C_4F_8 and CHF_3

G. A. Hebner

Sandia National Laboratories

Albuquerque NM, 87185-1423

Abstract

Laser induced fluorescence was used to measure the spatially resolved CF, CF_2 and SiF radical density in inductively driven discharges containing fluorocarbon gases. Measurements of the spatially resolved CF density were performed in C_2F_6 and CHF_3 containing discharges as functions of inductive power, pressure and bias condition on a silicon substrate. In addition, CF rotational temperatures were calculated, assuming saturated spectra. Measurements of the spatially resolved CF_2 and SiF density were performed in C_4F_8, C_2F_6 and CHF_3 containing discharges as functions of inductive power, pressure and bias condition. SiF rotational temperatures were also estimated. As the induction coil power was increased, the SiF density in the center (r = 0 cm) increased while the CF_2 density decreased and the CF density slightly decreased. In all cases, the radical density in the center of the glow increased with pressure changes from 5 to 30 mTorr while changes in the bias power had little influence on any of the measured radical densities. The spatial distribution of the CF and SiF density peaked in the center of the discharge. The CF_2 density had a local maximum in the center of the plasma with a

DISCLAIMER

DISCLAIMER

Portions of this document may be illegible in electronic image products. Images are produced from the best available original document.

decreasing density at the edge of the glow. However, the CF_2 density outside the glow region was a factor of 2 – 6 higher than the density inside the glow region, depending on the gas. CF and SiF rotational temperatures were between 450 and 750 K.

I. Introduction

Discharges containing fluorocarbon gases such as C_2F_6, C_4F_8 and CHF_3 are commonly used in a number of materials processing recipes. For example, in silicon dioxide etching for microelectronic feature definition, these gases serve as rich sources of atomic fluorine to remove the silicon dioxide as well as $C_xH_yF_z$ radicals that provide sidewall passivation and protection. When using these gases, anisotropic oxide etching has been shown to result from a critical balance between etching due to atomic fluorine, and sidewall and photoresist protection due to $C_xH_yF_z$ radicals depositing on the surface. In addition to standard silicon oxide etch processing applications, the addition of fluorocarbon gases to the plasma to produce a selective polymer coating on the surface is now being applied to a number of other processes. For example, recent advances in the processing of low dielectric constant materials (low-k) suggest that small additions of fluorocarbon gases to produce $C_xH_yF_z$ radicals for surface and sidewall protection and passivation may be critical to anisotropic etching of these next-generation materials. In addition, some processing recipes now quickly alternate between a pure etch mode, using a gas such as SF_6, and a surface protection layer deposition mode using gases such as C_4F_8. Using this alternating etch / deposition mode, it is possible to produce a number of structures such as micromechanical machine parts.

One method used to maximize tool throughput and minimize processing time is to increase the etch rate by increasing the bulk plasma charge density and hence, the ion flux to the surface. However, in high electron density plasma reactors such as inductively coupled plasmas (ICP) and electron cyclotron resonance (ECR) microwave driven plasmas, it is very easy to excessively dissociate the $C_xH_yF_z$ species and generate a

fluorine rich, CF_x polymer poor environment that is detrimental to a stable, anisotropic etch process. Thus there is a need to understand the gas and surface phase chemistry in high-density plasma systems in order to exploit fully the potential of high-density plasmas for stable, high throughput processes. A major component of the gas and surface phase chemistry models are the fluorocarbon dissociation products CF and CF_2. These species, in addition to higher molecular weight radicals, play a major role in the establishment and characteristics of the quasi stable polymer coating on the surface. In addition, SiF is produced from either ion bombardment of the surface or the plasma dissociation of SiF_x etch products that are removed from the surface. Thus it provides an indication of the silicon removal rate and indirectly the surface polymer coverage.

CF_x and SiF_x radical species measurements have been made in a number of discharge configurations using several different techniques. Infrared diode laser absorption measurements in the 10 μm region have been used to measure the line integrated CF_x (x = 1-3) density in parallel plate, ECR and ICP discharge configurations.[1,2,3,4] .Since the absorption line strengths for these transitions are known, it is possible to derive absolute, line integrated densities. If the spatially resolved density and temperature variation is known from some other technique, than it is possible to combine the results to give spatially resolved, absolute densities.[4] SiF and SiF_2 radicals have been measured in SiF_4 discharges using infrared absorption techniques but have not been observed in fluorocarbon etching systems, likely due to the lower density and partial pressure.[5,6] However, broadband UV absorption has been used to detect SiF_2 in fluorocarbon discharges.[7]

Laser induced fluorescence has been used to detect CF, CF_2, SiF and SiF_2 in processing discharges.[8,9,10,11,12,13,14,15,16,17] These measurements have been used to determine the relative radical density in a number of fluorocarbon containing discharges, mostly in parallel plate systems and some ECR systems. LIF is a very flexible, spatially selective technique that can provide detailed information on important discharge processes related to both the surface and gas phase. For example, the influence of bias voltage and electrode impedance on the spatial distribution of CF_2 in CF_4 / O_2 and C_2F_6 / O_2 has recently been demonstrated.[18,19] Spatially resolved LIF in the direction perpendicular to the rf biased surface has also been used to examine the surface flux rates of CF and CF_2 for a number of plasma conditions and surface conditions, again in parallel plate systems.[8,9] Time dependent loss processes of CF and CF_2 have also been examined in pulse modulated systems.[11,12,20,21,22] Surface reaction rates and sticking probabilities have also been measured using LIF.[23] Finally, the absolute density of some radical species can be determined by correlation with known concentrations of a stable molecule[24] or recently, cavity ringdown spectroscopy.[25]

In addition to optical techniques, a number of groups have used mass spectrometer systems to measure the neutral and ion species in the plasma.[26,27,28,29] While positive ion species are fairly straightforward to detect and interpret, neutral species can be more problematic since they must first be ionized using an electron beam. This can result in radical dissociation within the ionizer, which in principle can be corrected for in some cases, but often clouds the direct interpretation of the data. However, recently data has been presented that used a modified mass spectrometer system to observe relatively

fragile C_xF_y species with x up to 10.[28] Mass spectrometer heads can also perturb the plasma by their presence, and do not provide spatial information.

The goal of this work was to characterize the spatially resolved CF, CF_2 and SiF density in the inductively coupled GEC rf reference cell. The data will be used to determine the scaling of the radical species with discharge parameters, spatial distributions, gas temperatures, and to provide data to validate models. However, our broader goal is to determine as many of the characteristics of ICP discharges in the GEC rf reference cell as possible. Such a complete characterization greatly aids in understanding and modeling the extremely complex chemistry of fluorocarbon containing discharges. Due to the very complex gas and surface chemistry in these gases and the myriad of potential plasma species, experiments must often be coupled with sophisticated models to begin to fully identify the important mechanisms and gaps in our understanding of the fundamental physics. Towards that goal, this work is complemented by previous measurements of the electron density, temperature, and negative ion density in C_2F_6 and CHF_3.[30] Recent measurements of the electron and negative ion density in C_4F_8 have also been performed; those densities are similar to the values in C_2F_6 and will be reported elsewhere.

II. Experimental configuration

Experiments were performed in a Gaseous Electronics Conference (GEC) rf reference cell which was modified to include an inductively coupled plasma (ICP) source.[31, 32] As shown in Fig. 1, the water-cooled induction coil was constructed from 3.2 mm diameter copper tubing which was wound into a five-turn planar coil 11 cm in

diameter. In this work, the coil was excited at 13.56 MHz. The coil was separated from the plasma by a 1-cm-thick fused silica window. The spacing between the window and the grounded lower electrode was 3.8 cm. For these experiments, the lower electrode was rf biased (13.56 MHz) and covered with a 6 inch diameter silicon wafer which was not clamped in place. The lower electrode was water cooled; however, the reactor was run with a discharge ($C_xH_yF_z$ or O_2) for 30 minutes to reach a steady-state temperature before any measurements were made. For these experiments an additional modification was made to the GEC chamber; a fused silica ring was clamped to the upper electrode assembly as shown in Fig. 1. The fused silica confinement ring served to stabilize and extend the operating parameter space of the fluorocarbon discharges. Without the ring in place, the discharge could only be sustained over a narrow range of power and pressure. The ring had an inner diameter of 4.5 inches, outer diameter of 6.5 inches and a thickness of 0.75 inches. In addition, the standard stainless steel ICP window holder was replaced by an anodized aluminum holder so that the materials in contact with the plasma would more closely resemble those found in commercial tools. Measurements of the induction coil and bias voltages and currents, as well as electron and negative ion densities for C_2F_6 and CHF_3 gases in this geometry have been previously reported.[30] Electron and negative ion density measurements in C_4F_8 have been performed and are similar to C_2F_6 in some cases.

Laser induced fluorescence was used to measure the CF, CF_2 and SiF density. The excitation laser was aligned through the chamber, parallel to the lower electrode surface and centered approximately 0.7 cm above the surface. A pulsed laser (Contiuum Sunlite or Quantel dye with frequency conversion) was used with pulse lengths of

approximately 5 ns and attenuated, unfocused, beam energies on the order of 100 μJ. The CF density was monitored using two different wavelengths since two different laser systems were used. To measure the CF density in the center of the plasma and the spatial distributions, a pulsed dye laser was used to excite the A – X (1,0) bandhead at 223.8 nm with observation of the fluorescence at 267 nm (1,6). To measure the CF rotational temperatures, the A – X (0,0) system was excited at approximately 233 nm and fluorescence was observed at 255 nm (0,3). CF_2 density was monitored by exciting the X – A (0,0,0 – 0,5,0) manifold at 251.9 nm and observing the fluorescence at 280 nm (0,6,0). SiF density was determined by exciting the X – B (0,1) bandhead at 288.05 nm and observing fluorescence at 296.7 nm (1,1). In all cases, the laser wavelength as well as the monochromator wavelength were scanned to insure that the appropriate radical spectrum was observed.

As shown in Fig. 2, LIF was observed at a right angle to the pump beam using two different detection systems. The first utilized a lens to focus the LIF into the entrance slit of a monochromator. Fluorescence intensity and lifetime was determined using a photomultiplier tube and a digitizing scope. This detection system had the advantage of monitoring the relatively weak radical density with high spatial resolution. Since our GEC chamber can be translated, this system was also used to insure that the LIF lifetime did not vary with radial position as well as recording the radial variation of the radial density over a limited range of radial positions ($r < 6$ cm). In most cases, approximately 256 laser pulses were averaged.

The second system used a gated, intensified CCD camera, bandpass filter and UV lens to measure the spatial variation of the LIF. The camera was aligned at a slight angle

with respect to the 8 inch view port on the GEC reference cell to view the LIF from the center of the plasma to beyond the glow region. A ruler was placed in the chamber to optimize the lens focus and record the spatial position as a function of camera pixel. Since the beam was of finite size, camera pixel averaging was used to generate density profiles as a function of radial position. For this study, no attempt was made to measure the density variation as a function of height above the surface. The intensifier gate width was set to 150 ns and approximately 1000 laser pulses were averaged. The plasma induced emission (PIE) was subtracted in all cases. The spatial variations obtained using the lens / monochromator system and the CCD camera system were identical over the range of radial positions examined.

III. Results and Discussion

A. CF

The rotational temperature for CF was measured in C_2F_6 for several plasma conditions and radial positions. For these measurements, the laser was tuned over a limited range of rotational lines that exhibited large changes in relative amplitude with rotational temperature. Figure 3 shows several calculated and measured spectra. The top figure (a) shows the calculated CF spectra over a relatively large spectral range with the range measured in detail marked by the bracket. Spectra in plots (b), (c) and (d) are three examples of calculated rotational spectra. The spectra were calculated assuming fully saturated LIF conditions. In practice, there was a very weak dependence of LIF intensity on laser power since it is often difficult to fully saturate the molecular transitions. An example of a measured spectrum is shown in Fig. 3(e). Spectra were calculated for every

50 K and then an optimizing program was used to compare the measured and calculated spectra to determine the best rotational temperature using a single scaling parameter for the amplitude. Over the range of rotational temperatures determined by this work, the CF densities measured by exciting the bandhead would vary approximately 15 percent since the A – X (1,0) band head strength was not a strong function of temperature.

Rotational temperatures as functions of induction coil power, pressure and bias power are shown in Fig. 4. The majority of this data was obtained at r = 0 cm although two points, marked on the graph as r = 5 cm, were obtained at the edge of the glow. The relative uncertainty in the temperature dependent fits to the data can be deduced from the multiple spectra and derived temperatures that were obtained at 200 W induction coil power, 10 mTorr and 20 W bias power. These data show an increase in CF temperature with induction coil power. Such an increase could be the result of plasma heating of ions that subsequently dissociate to form CF, or less likely, molecular charge exchange. The data obtained at r = 5 cm did not show a significantly different CF temperature even though the CF density and the electron density were a factor of 2 lower than the values in the center of the plasma. To within the uncertainty in the data, rotational temperature was not a function of pressure. Thus energy loss or cooling of the CF or its precursors due to collisions with neutral or other species does not appear to be a significant factor. As the rf bias power was increased, the measured CF temperature appears to decrease slightly. The data points at rf bias powers of 0 and 100 W were repeated multiple times to check this observation. The mechanism responsible for this slight decrease is unknown. If more CF was being sputtered from the surface as the bias power was increased, which is likely at a slightly elevated temperature of 400 K, then the decrease

could be due to cold CF from the surface mixing with hot CF in the plasma resulting in a colder CF distribution in the gas phase. However, as will be discussed below, the total CF density did not change appreciably with bias power. One speculation might be that as the bias power is increased, the increased bias power, which is a reasonable fraction of the induction coil power, results in a decreased CF density due to electron driven dissociation. Our previous measurements showed an increase in electron density with bias power increase.[30] But the increased bias power also results in an increase in the sputtered CF from the polymer coated surface. Such a shift in the source of CF could result in a decreased CF temperature if the net CF in the plasma is produced by these two sources.

In general, the temperatures reported here are much higher than room temperature, in contrast to measurements by Haverlag et al obtained in a parallel plate reactor.[2] They reported CF_4 temperatures, obtained by line integrated diode laser measurements, that were at most 360 K in CF_4 and CHF_3 containing parallel plate driven plasmas. However, our higher CF temperature is consistent with our previous measurements in this discharge geometry of argon and chlorine temperatures of approximately 800 K.[33,34] The differences are likely due to the higher electron density in the GEC ICP geometry due to higher input power per unit volume as well as enhanced dissociation and ion heating. In addition, as will be shown below, the line-integrated measurement may be including stable radicals that are outside the plasma region and which may be colder than the plasma heated radicals.

CF densities in the center of the plasma for discharges containing C_2F_6 and CHF_3 as functions of induction coil power, pressure and bias power are shown in Fig. 5. The

center point about which the experimental conditions were changed was 200 W of induction coil power, 10 mTorr, 20 W bias power and 10 sccm flow rate. These measurements were obtained using the lens / monochromator system at r = 0 cm and a height of 0.7 cm above the silicon wafer. Fluorescence lifetime was approximately 29 ns and did not vary with plasma condition or radial position. The relative density of CF in C_2F_6 was a factor of 1.5 – 2 higher than in CHF_3.

As the inductive source power was increased from 100 to 400 W, the CF density decreased approximately a factor of two in both gases. The measured CF density is the result of a number of possible production and loss mechanisms that can be related to both bulk and surface chemistry. For example, CF could be produced by electron dissociation of larger CF_x species or sputtered from the surface, and lost by electron driven dissociation or reactions at the surface. Based upon the gas temperature determined from the CF rotational temperature measurements and using the ideal gas law, it is possible to calculate the change in density, for constant pressure, that would result from only an increase in temperature. Those curves, scaled by a single factor to account for the arbitrary density are shown as the solid lines in Fig. 5. Thus the majority of the change in CF density can be attributed to a change in gas temperature, in spite of a factor of 8 change in the electron density over this same parameter space.[30] Such a curve would be expected if the major production and loss terms for CF were directly proportional to the electron density and constant. In addition, it appears that CF may not be a major precursor species to the formation of the negative ions in the plasma since the negative ion density was observed to peak strongly for inductive powers of approximately 250 W and the CF density appears to have no major changes over this power range.[30]

The CF density in C_2F_6 and CHF_3 increased approximately linearly when the pressure was increased from 5 to 30 mTorr. The linear increase in the CF density indicates that the rates of the various dissociation mechanisms to produce the gas phase CF scale with feed gas pressure. Over this parameter space, the CF temperature did not change significantly so corrections due to gas heating are minimal. Finally, over this same range of pressure, the electron density was constant to slightly decreasing in the case of C_2F_6 while the negative ion density was relatively constant; consistent with the observation above that CF may not be a major precursor species to the negative ion formation.

Changes in the rf bias voltage on the silicon wafer substrate had little influence on the CF density for either gas. Even when the rf bias power was increased to 300 W, as shown in Fig. 6 for the case of C_2F_6, the CF density was constant with rf bias power. In addition to rf bias power, the voltage and current at the wafer surface for the fundamental (13.56 MHz) and the second harmonic increase with bias power, as shown. Our previous electron density measurements showed that the electron density increased approximately 50 and 80 percent for increased bias power from 0 to 150 W in CHF_3 and C_2F_6, respectively.[30] Thus the CF density appears to be constant despite an increase in both the number of ions striking the surface and the energy of the ions. As suggested above, this could be due to a balance between increased CF loss due to electron driven dissociation processes and increased C_xF_y polymer sputtering from the surface. The sputtered material is unlikely to be just CF but rather an ill-defined mixture of C_xF_y species that may be in turn be dissociated by the plasma to form CF. Since both production and loss processes are proportional to electron density, the net effect may be a relatively constant

CF density. Changes in the spatial distribution of CF above the surface could possibly be used to explore this argument.

The spatial distribution of CF in C_2F_6 and CHF_3 discharges are shown in Fig. 7 and 8, respectively. For the case of C_2F_6, the CF density was a maximum in the center of the plasma region and decreased below the fused silica confinement ring and outside the glow region. In general, the relative shape of the distribution did not change with discharge condition; even the radial distribution did not change significantly with rf bias. For the case of CHF_3, the spatial distributions of CF was much flatter than in C_2F_6 and the CF density appears to be significant out to the walls of the GEC chamber (r = 14 cm). The 1 cm long undulations in the density are the result of our data smoothing routine. The significant differences in the two gases may be due to large differences in the CF diffusion coefficient[21,22] or due to changes in the gas phase loss rate for CF in the two gases.

B. CF_2

CF_2 densities in the center of the plasma for discharges containing C_4F_8, C_2F_6 and CHF_3 as functions of induction coil power, pressure and bias power are shown in Fig. 9. The center point about which the experimental conditions were changed was 200 W of induction coil power, 10 mTorr, 20 W bias power and 10 sccm flow rate. For these plots, the data for each gas was normalized to a density of one at the center point of the experimental conditions. The relative density of the CF_2 in the three gases was 1.0 for C_4F_8, 0.3 for C_2F_6 and 0.1 for CHF_3. Thus the CF_2 density in C_4F_8 was a factor of 10 higher than the density in CHF_3. These measurements were obtained using the lens /

monochromator system at r = 0 cm and a height of 0.7 cm above the silicon wafer. Fluorescence lifetime was approximately 60 ns and did not vary with plasma condition or radial position.

As the induction coil power was increased, the normalized CF_2 density decreased by the same amount for all three gases investigated. Based upon the gas temperature determined from the CF rotational temperature measurements and using the ideal gas law, it is possible to calculate the change in density, for constant pressure, that would result from an increase in temperature. That curve, normalized to the point at 200 W, is shown as the solid line. Thus the majority of the change in CF_2 density can be attributed to a change in gas temperature, in spite of a factor of 8 change in the electron density over this same parameter space. Such a curve would be expected if the major production and loss terms for CF_2 were directly proportional to the electron density and constant. As discussed above, this same relationship was also observed for the CF density in the center of the plasma. Like the CF density, it also appears that CF_2 may not be a major precursor species to the formation of the negative ions in the plasma since the negative ion density was observed to strongly peak for inductive powers of approximately 250 W and the CF_2 density appears to have no major changes over this power range.[30]

Increasing the chamber pressure resulted in an increased CF_2 density at higher pressures. When the pressure was increased from 5 to 30 mTorr, the CF_2 density in C_4F_8 increased linearly. However, the CF_2 density in C_2F_6 at higher pressures showed indications of saturation while the radical density in CHF_3 was relatively constant above 20 mTorr. Over this same parameter space, the CF temperature did not change significantly so corrections due to gas heating are minimal. In addition, the electron

density in CHF_3 was relatively constant while in C_4F_8 and C_2F_6 the electron density decreased by a factor of approximately two. Thus despite a decrease in the electron density with pressure, the CF_2 density in C_2F_6 and C_4F_8 was higher and did not saturate with pressure. The different trends with pressure for the three gases may be due to the formation of different gas and surface phase heavy polymers.[27,28] The formation of larger C_xF_y polymers is more likely in feedgases with smaller C/F ratios. Heavier polymers would provide more pathways for CF_2 formation by electron dissociation of C_xF_y precursors, as well as influencing plasma properties such as electron temperature.

Changes in the rf bias power had minimal influence on the measured CF_2 density for all the gases studied. For rf bias powers up to 200 W, the CF_2 density was relatively constant. As with the discussion of the CF density above, the relatively constant CF_2 density is likely the result of several competing processes. All other factors being constant, the measured decrease in CF gas temperature measured over this range would result in an increased CF_2 density. However, since the CF_2 density does not decrease, there is some process removing the CF_2 as the rf bias is increased. That removal may be electron driven dissociation of the CF_2 since the additional power input into the plasma by the biased surface results in an increase in electron density. Changes in the spatial distribution of CF_2 above the surface could also possibly be used to explore this argument.

Spatially resolved CF_2 densities in C_2F_6, CHF_3 and C_4F_8 are shown in Figs. 10, 11 and 12, respectively, as functions of induction coil power, pressure and bias power. In addition, a representative spatially resolved, plasma induced emission (PIE) profile from CF_2 is shown as is the location of the quartz confinement ring. In general, the PIE is

roughly the same shape as the spatially resolved electron density, as determined by a Langmuir probe, although the electron density tends to be more Gaussian. The main feature in all of these plots is the large CF_2 density outside the plasma region. Unlike the spatially resolved CF density discussed above, the CF_2 density is significant and increasing as a function of larger radial position. Due to the geometry of the GEC reference chamber, the plasma volume is only a small fraction of the total chamber volume. Thus the total CF_2 density outside the glow region is significant. If the source of the CF_2 outside the glow region is strictly due to the plasma, the CF_2 has a relatively long lifetime and small surface loss rate. These measurements also suggest that line integrated diode laser measurements of CF_2 densities may not be capturing the CF_2 density in the bulk plasma region if there is dead space in the absorption path. No attempt was made in this work to measure the time dependent build up of the CF_2 in the region outside the plasma by pulse modulating the plasma.

There are interesting similarities and differences in the spatial profiles for each of the gases. In the case of C_2F_6 and CHF_3, the CF_2 density is only slightly higher in the center of the plasma, r = 0 cm, than in the area under the fused silica confinement ring. The relatively flat profile in the plasma region supports the idea that the surface production / loss rates and gas phase production / loss rates are relatively local. There is not a large radial gradient of CF_2 due to net radical flow from the plasma region to the region outside the plasma. However, the CF_2 density in the center of the C_4F_8 plasma is comparable to the density outside the plasma region and there is a relatively large gradient in CF_2 density from r = 0 cm to the edge of the glow region. This gradient suggests several mechanisms such as large CF_2 production rates in the center of the

discharge, where the electron density is highest, spatially varying electron temperatures or surface loss to the wafer. In addition to the plasma pumping CF_2 into the region outside the glow, the relatively high CF_2 density in the region outside of the glow can act as a source term for CF_2 back into the plasma. As with the case of CF, there was not a large change in the CF_2 radial profile with bias condition.

C. SiF

SiF densities in the center of the plasma for discharges containing C_4F_8, C_2F_6 and CHF_3 as functions of induction coil power, pressure and bias power are shown in Fig. 13. The center point about which the experimental conditions were changed was 200 W of induction coil power, 10 mTorr, 20 W bias power and 10 sccm flow rate. The SiF density for each gas has not been normalized. Thus the SiF density is approximately 3 times as large in C_2F_6 as in C_4F_8, for example. These measurements were obtained using the lens / monochromator system at r = 0 cm and a height of 0.7 cm above the silicon wafer. Fluorescence lifetime was approximately 11 ns and did not vary with plasma condition or radial position. As in the case of CF, several complete rotationally resolved SiF spectra were obtained for the 0 – 1 vibrational transition of the B – X system. However, in many parts of the spectra, the rotational spacing of the SiF rotational lines was less than our laser linewidth. Thus it was difficult to resolve individual rotational features to derive a rotational temperature. However, we did fit the envelope of the spectra to calculated spectra, assuming saturated LIF conditions. Those temperatures were comparable to the values measured for CF, namely 500 – 600 K for plasma conditions of 200 W induction coil power, 10 mTorr and 20 W rf bias. The relatively

weak LIF from SiF made spatial measurements difficult. A limited number of spatial profiles indicated that SiF peaked in the center of the plasma, and significantly decreased at edge of the glow. No SiF was observed outside the plasma region.

Unlike the CF and CF_2 densities in the center of the plasma, increasing the induction coil power resulted in an increase in the SiF density. If the gas phase SiF results from either direct sputtering from the wafer surface or the electron dissociation of SiF_x etch species, the SiF density should scale with the ion flux to the surface or the electron density. The solid lines are fits assuming that the gas phase SiF density would increase in proportion to the measured linear increase in electron density with induction source power, and decrease due to gas heating, at constant pressure (using a linear fit to the CF temperature data). The only variable parameter in the fit was a single amplitude-scaling factor since the SiF density units were arbitrary. In general, the fits to the data capture the major trends for each gas, supporting the contention that the SiF density is directly proportional to the electron density (and hence the ion density), reduced by the gas temperature. However, discrepancies to the fits at high and low induction coil powers show that this simple view of the SiF density is not quite correct, as one would expect in such a chemically complicated system.

Unlike the CF and CF_2 data, an increase in the pressure did not result in a linear increase in the SiF density for all the gases. The SiF density increased monotonically with pressure for CHF_3. However for C_2F_6, the SiF density increased for pressures up to approximately 10 mTorr and was constant to slightly decreasing at higher pressures. For the case of C_4F_8, the SiF density was relatively independent of pressure. The relatively low SiF density in C_4F_8 is likely due to the highly polymerizing nature of C_4F_8 coating

the surface and reducing the silicon etch rate. At higher pressures, C_2F_6 also becomes more polymerizing and more effectively covers the surface. By extension, CHF_3 does not coat the surface as quickly or with as high a flux since its C / F atomic density is smaller and the H is believed to effectively scavenge F atoms that would produce the CF_x coating on the surface.

Changes in the SiF densities with rf bias power were somewhat gas dependent. For the case of C_2F_6, the SiF density did not strongly depend on the bias power. If the gas temperature decreased with an increase in bias power, then the flat SiF density represents a net increase in the flux of SiF from the surface, as would be expected with an increase in bias. The fact that the SiF density does not go up even more may be due to enhanced dissociation due to the increased electron density, as discussed above for CF and CF_2. In the case of CHF_3, an increase in bias power did not have a significant influence on the SiF density. This would be expected if the CF_x film created on the surface by the CHF_3 was not very thick or reactive. For C_4F_8 feed gas, the SiF density appears to slightly increase with rf bias. This may be due to the increased ion bombardment at the higher bias powers (voltages) opening up surface sites or freeing SiF_x species from the surface. The relative density and power scaling of the SiF density is also consistent with C_4F_8 creating more CF_x polymer surface layer than C_2F_6 or CHF_3.

IV. Summary

Laser induced fluorescence was used to measure the spatially resolved CF, CF_2 and SiF radical density in inductively driven discharges containing C_4F_8, C_2F_6 and CHF_3. CF rotational temperatures were determined by fitting the measured spectra to calculated

spectra, assuming saturated LIF conditions. These data show an increase in CF temperature with induction coil power. Such an increase could be the result of plasma heating of ions that subsequently dissociate to form CF, or less likely, charge exchange. The data obtained at r = 5 cm did not show a significantly different CF temperature even though the CF density and the electron density were a factor of 2 lower than the values in the center of the plasma. To within the uncertainty in the data, rotational temperature was not a function of gas pressure. Thus energy loss or cooling of the CF due to collisions with neutral or other species does not appear to be a significant factor. As the rf bias power was increased, the measured CF temperature appeared to slightly decrease.

The decrease in the CF and CF_2 density in the center of the plasma with increased induction coil power could be fit assuming that the radical density decreased by gas heating and the production / loss terms were all proportional to electron density and constant. The reasonable fit, despite the factor of 8 change in the electron density over the measured change in power, indicates that the majority of the surface and gas phase production / loss rates likely scale with electron density. In all cases, increasing the pressure resulted in an increase in the CF and CF_2 density, although for higher pressures, the CF_2 density appears to saturate, possibly due to gas dependent, enhanced surface polymerization. The gas phase CF and CF_2 density did not appear to strongly depend on bias power. Our data indicates that both CF and CF_2 may not be a major precursor species to the formation of the negative ions in the plasma since the negative ion density was observed to strongly peak for inductive powers of approximately 250 W and the CF and CF_2 density appear to have no major changes over this power range.

LIF was used to measure the spatial distribution of the radical species. For the case of C_2F_6, the CF density had a maximum in the center of the plasma region and decreased below the fused silica confinement ring and outside the glow region. In general, the relative shape of the distribution did not change with discharge condition. Even the radial distribution did not change significantly with rf bias. For the case of CHF_3, the spatial distributions of CF were much flatter than in C_2F_6 and the CF density appears to be significant out the walls of the GEC chamber (r = 14 cm). Unlike CF, the main feature of the CF_2 spatial distributions was the large CF_2 density outside the plasma region. In most cases, the CF_2 density had a local maximum in the center of the plasma with a decreasing density at the edge of the glow. However, the CF_2 density outside the glow region was a factor of 2 – 6 higher than the density inside the glow region, depending on the gas. The different CF_2 spatial distribution in C_4F_8 compared with C_2F_6 and CHF_3 indicates additional production / loss terms for CF_2.

LIF measurements of SiF showed that unlike the CF and CF_2 densities in the center of the plasma, increasing the induction coil power resulted in an increase in the SiF density. The SiF data was fit assuming that the gas phase SiF density would scale with the measured linear increase of electron density with inductive source power, and a density decrease due to gas heating, at constant pressure (using a linear fit to the CF temperature data). In general, the fits to the data capture the major trends for each gas; supporting the contention that the SiF density is directly proportional to the electron (and hence the ion density), reduced by the gas temperature. However, discrepancies to the fits at high and low induction coil powers show that this simple view of the SiF density is not quite correct, as one would expect in such a chemically complicated system. Changes

in the SiF density with pressure and bias power were also gas dependent, likely due to the change in the surface polymer coating. Spatial profiles SiF density showed that it peaked in the center of the plasma. Fits to the rotational manifold indicated that the SiF rotational temperature were 500 – 600 K, consistent with CF.

V. Acknowledgments

The author thanks P. Ho, J. Johannes, I. Abraham, C. Woods and H. Anderson for many helpful discussions. The technical assistance of T. W. Hamilton is gratefully recognized. This work was performed at Sandia National Laboratories and supported by SEMATECH and the United States Department of Energy (DE-AC04-94AL85000). Sandia is a multiprogram laboratory operated by Sandia Corporation, a Lockheed Martin Company, for the U. S. Department of Energy.

Figure Captions

Fig. 1 Cross section view of the GEC rf reference chamber showing the location of the fused silica confinement ring and rf biased electrode.

Fig. 2 Experimental configuration showing the location of the two laser induced fluorescence detection systems.

Fig. 3 Partial spectra showing calculated CF rotational line intensities. Plot (a) is an larger wavelength range and shows the location of the subplots by the bracket. Plots (b), (c) and (d) are subsets of (a) as a function of rotational temperatures of 700, 500 and 300 K. Plot (e) is an example of a measured CF spectra. C_2F_6 was used with 200 W of induction coil power, 10 mTorr pressure, 20 W of rf bias power and 10 sccm flow rate.

Fig. 4 CF rotational temperatures in C_2F_6 as functions of induction coil power, pressure and bias power. The common experimental parameters were 200 W of induction coil power, 10 mTorr pressure, 20 W of rf bias power and 10 sccm flow rate. Except for the two points noted by the arrows (r = 5 cm), the data was obtained in the center of the plasma (r = 0 cm).

Fig. 5 Relative CF density in C_2F_6 (●) and CHF_3 (▼)a functions of induction coil power, pressure, and rf bias power. The common experimental parameters were 200 W of induction coil power, 10 mTorr pressure, 20 W of rf bias power and 10 sccm flow rate. The solid line is a fit showing the density decrease due to only gas temperature changes.

Fig. 6 Relative CF density, bias voltage at the wafer surface, and bias current at the wafer surface for the fundamental frequency (f_o = 13.56 MHz) and the second

harmonic as functions of the bias power. The gas was C_2F_6 with an induction coil power of 200 W and a pressure of 10 mTorr.

Fig. 7 Spatially resolved CF density in C_2F_6 as functions of induction coil power (a), pressure (b), and bias power (c). The common experimental parameters were 200 W of induction coil power, 10 mTorr pressure, 20 W of rf bias power and 10 sccm flow rate.

Fig. 8 Spatially resolved CF density in CHF_3 as functions of induction coil power (a), pressure (b), and bias power (c). The common experimental parameters were 200 W of induction coil power, 10 mTorr pressure, 20 W of rf bias power and 10 sccm flow rate. The oscillations with one cm period in the density are due to the smoothing algorithm.

Fig. 9 Relative CF_2 density in C_4F_8 (●), C_2F_6 (▼) and CHF_3 (■)a functions of induction coil power, pressure, and rf bias power. The common experimental parameters were 200 W of induction coil power, 10 mTorr pressure, 20 W of rf bias power and 10 sccm flow rate. Data for different gases was scaled to one at the common operating point. The relative density of the CF_2 in the three gases was 1.0 for C_4F_8, 0.3 for C_2F_6 and 0.1 for CHF_3. The solid line is a fit showing the density decrease due to only gas temperature changes.

Fig. 10 Spatially resolved CF_2 density in C_2F_6 as functions of induction coil power (a), pressure (b), and bias power (c). Plot (a) also shows an example of the spatially resolved plasma induced emission at 280 nm while plot (c) shows the location of the fused silica confinement ring. The common experimental parameters were

200 W of induction coil power, 10 mTorr pressure, 20 W of rf bias power and 10 sccm flow rate.

Fig. 11 Spatially resolved CF_2 density in CHF_3 as functions of induction coil power (a), pressure (b), and bias power (c). Plot (a) also shows an example of the spatially resolved plasma induced emission at 280 nm while plot (c) shows the location of the fused silica confinement ring. The common experimental parameters were 200 W of induction coil power, 10 mTorr pressure, 20 W of rf bias power and 10 sccm flow rate.

Fig. 12 Spatially resolved CF_2 density in C_4F_8 as functions of induction coil power (a), pressure (b), and bias power (c). Plot (a) also shows an example of the spatially resolved plasma induced emission at 280 nm while plot (c) shows the location of the fused silica confinement ring. The common experimental parameters were 200 W of induction coil power, 10 mTorr pressure, 20 W of rf bias power and 10 sccm flow rate.

Fig. 13 Relative SiF density in C_4F_8 (▲), C_2F_6 (●) and CHF_3 (■)a functions of induction coil power, pressure, and rf bias power. The common experimental parameters were 200 W of induction coil power, 10 mTorr pressure, 20 W of rf bias power and 10 sccm flow rate. The solid line is a fit showing the density scaling if the SiF increased linearly with the measured electron density, corrected for the decrease in density due to gas heating.

References

[1] K. Miyata, M. Hori and T. Goto, Jpn. J. Appl. Phys., 36, 5340 (1997).

[2] M. Haverlag, E. Stoffels, W. W. Stoffels, G. M. W. Kroesen and F. J. de Hoog, J. Vac. Sci. Technol. A 14, 380 (1996).

[3] K. Miyata, M. Hori and T. Goto, J. Vac. Sci. Technol A 14, 2343 (1996).

[4] M. Nakamura, H. Nakayama, M. Ito, M. Hori, T. Goto, A. Kono, I. Akihiro, N. Ishii, Jpn. J. Appl. Phys., Part 1 38 (12A), L1469 (1999).

[5] K. Tanaka, Y. Akiyama and T. Tanaka, J. Mol. Spec. 137, 55 (1989).

[6] G. L. Caldow, C. M. Deeley, P. H. Turner and I. M. Mills, Chem. Phys. Lett., 82, 434 (1981).

[7] J. P. Booth, G. Cunge, F. Neuilly and N. Sadeghi, Plasma Sources Sci. Technol. 7, 423 (1998).

[8] G. Cunge and J. P. Booth, J. Appl. Phys. 85, 3952 (1999).

[9] J. P. Booth, G. Cunge, P. Chabert and N. Sadeghi, J. Appl. Phys. 85, 3097 (1999).

[10] W. T. Conner and H. H. Sawin, Appl. Phys. Lett. 60, 557 (1991).

[11] C. Suzuki, K. Sasaki and K. Kadota, J. Appl. Phys. 82, 5321 (1997).

[12] A. D. Tserepi, J. Derouard, J. P. Booth and N. Sadeghi, J. Appl. Phys. 81, 2124 (1997).

[13] S. Vanhaelemeersch, J. Van Hoeymissen, D. Vermeylen and J. Peeters, J. Appl. Phys. 70, 3892 (1991).

[14] Y. Matsumi, S. Toyoda, T. Hayashi, M. Miyamura, H. Yoshikawa and S. Komiya, J. Appl. Phys. 60, 4102 (1986).

[15] G. Cunge, P. Chabert and J. P. Booth, Plasma Sources Sci. Tecnol. 6, 349 (1997).

[16] R. Walkup, Ph. Avouris, R. W. Dreyfus, J. M. Jasinski and G. S. Selwyn, Appl. Phys. Lett. 45, 372 (1984).

[17] C. W. Watson and K. G. McKendrick, Chem. Phys. 187, 87 (1994).

[18] M. A. Sobolewski and K. L. Steffens, J. Vac. Sci. Technol., A 17, 3281 (1999).

[19] K. L. Steffens and M. A. Sobolewski, J. Vac. Sci. Technol., A 17, 517 (1999).

[20] C. Suzuki and K. Kadota, Appl. Phys. Lett. 67, 2569 (1995).

[21] T. Arai, M. Goto, D. Takayama, T. Shimizu, M. Murakami, K. Horikoshi and H. Fujioka, Jpn. J. Appl. Phys. 34(10B), part 2, L-1392 (1995).

[22] T. Arai, M. Goto, D. Takayama, T. Shimizu and M. Murakami, Jpn. J. Appl. Phys. 33(7B), part 1, 4170 (1994).

[23] N. M. Mackie. V. A. Venturo and E. R. Fisher, J. Phys. B 101, 9425 (1997).

[24] G. Cunge, J. P. Booth and J. Derouard, Chem. Phys. Lett. 263, 645 (1996).

[25] J. P. Booth, G. Cunge, L. Biennier, D. Romanini and A. Kachanov, Chem. Phys. Lett. 317, 631 (2000).

[26] K. Teii, M. Hori, M. Ito, T. Goto, N. Ishii J. Vac. Sci. Technol., A 18, 1 (2000).

[27] R. Jayaraman, R. T. McGrath and G. A. Hebner, J. Vac. Sci. Technol., A 17, 1545 (1999).

[28] W. W. Stoffels, E. Stoffels and K. Tachibana, J. Vac. Sci. Technol. A 16, 87 (1998).

[29] J. K. Olthoff and Y. Wang, J. Vac. Sci. Technol., A 17, 1552 (1999).

[30] G. A. Hebner and P. A. Miller, Accepted J. Appl. Phys. July 2000.

[31] P. A. Miller, G. A. Hebner, K. E. Greenberg, P. D. Pochan and B. P. Aragon, J. Resch. Natl. Int. Standard. Technol 100, 427 (1995).

[32] P. J. Hargis Jr., K. E. Greenberg, P. A. Miller, J. B. Gerardo, J. R. Torczynski, M. E. Riley, G. A. Hebner, J. R. Roberts, J. K. Olthoff, J. R. Whetstone, R. J. Van Brunt, M. A. Sobolewski, H. M. Anderson, M. P. Splichal, J. L. Mock, P. Bletzinger, A. Garscadden, R. A. Gottscho, G. Selwyn, M. Dalvie, J. E. Heidenreich, J. W. Butterbaugh, M. L. Brake, M. L. Passow, J. Pender, A. Lujan, M. E. Elta, D. B. Graves, H. H. Sawin, M. J. Kushner, J. T. Verdeyen, R. Horwath and T. R. Turner, Rev. Sci. Inst. 65, 140 (1994).

[33] G. A. Hebner, J. Appl. Phys. 81, 578 (1997).

[34] G. A. Hebner, J. Appl. Phys. 80, 2624 (1996).

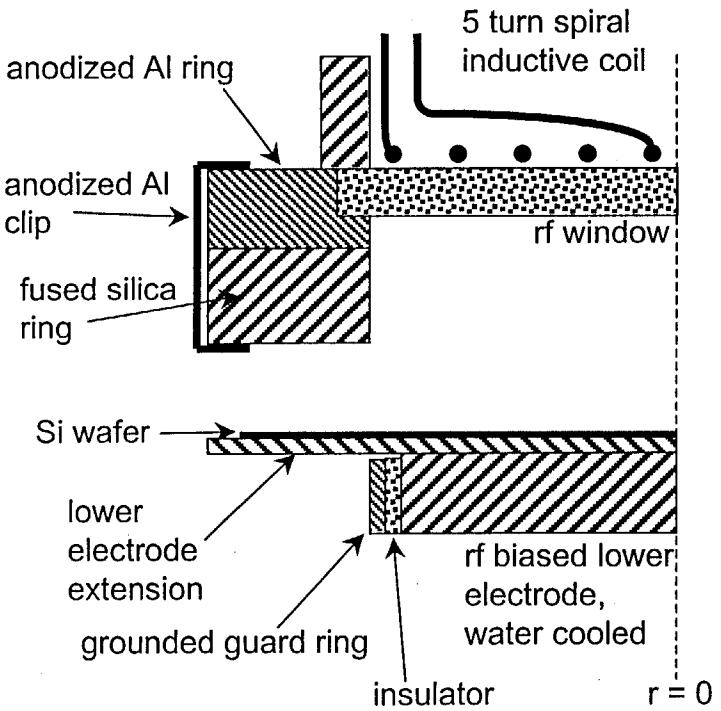
5 turn spiral
inductive coil
anodized Al ring
anodized Al
clip
rf window
fused silica
ring
Si wafer
lower
electrode
extension
grounded guard ring
insulator
rf biased lower
electrode,
water cooled
r = 0

Fig. 1
Hebner

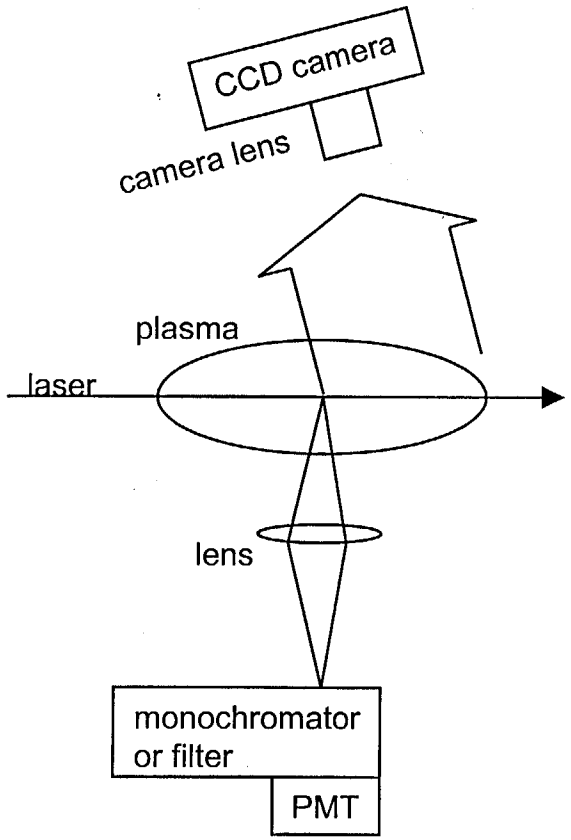
CCD camera
camera lens
plasma
laser
lens
monochromator
or filter
PMT

Fig. 2
Hebner

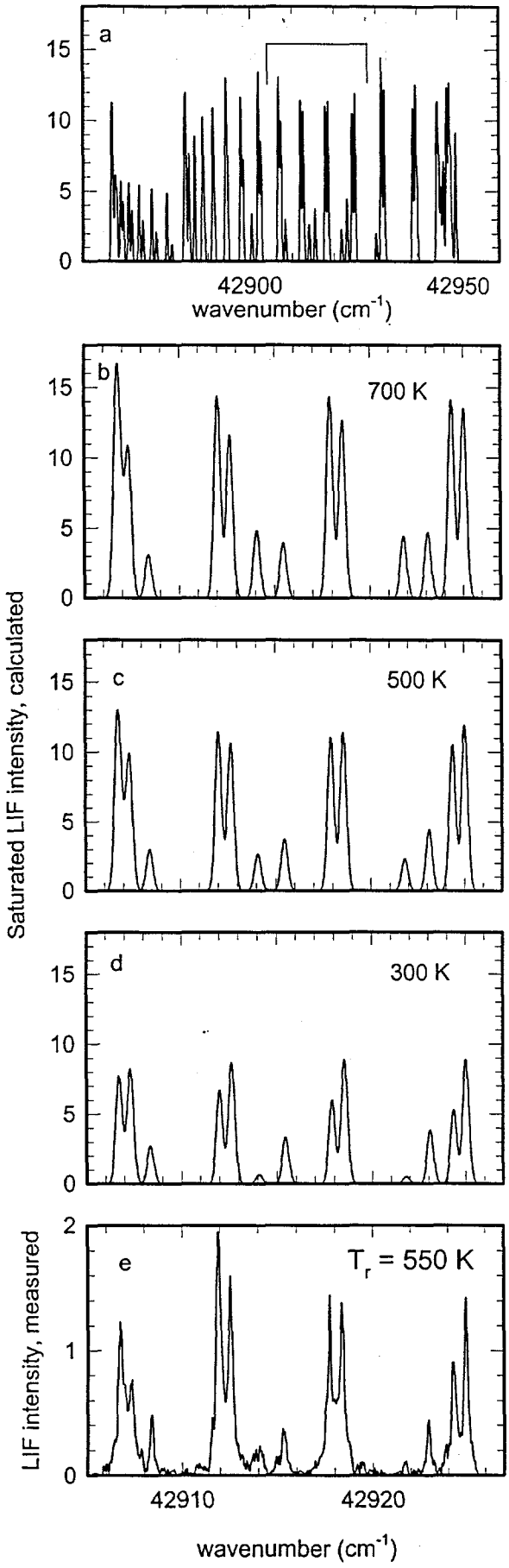
a
b
700 K
c
500 K
d
300 K
e
T_r = 550 K
15
10
5
0
2
1
42900
42950
42910
42920
wavenumber (cm^{-1})
Saturated LIF intensity, calculated
LIF intensity, measured

Hebner
Fig. 3

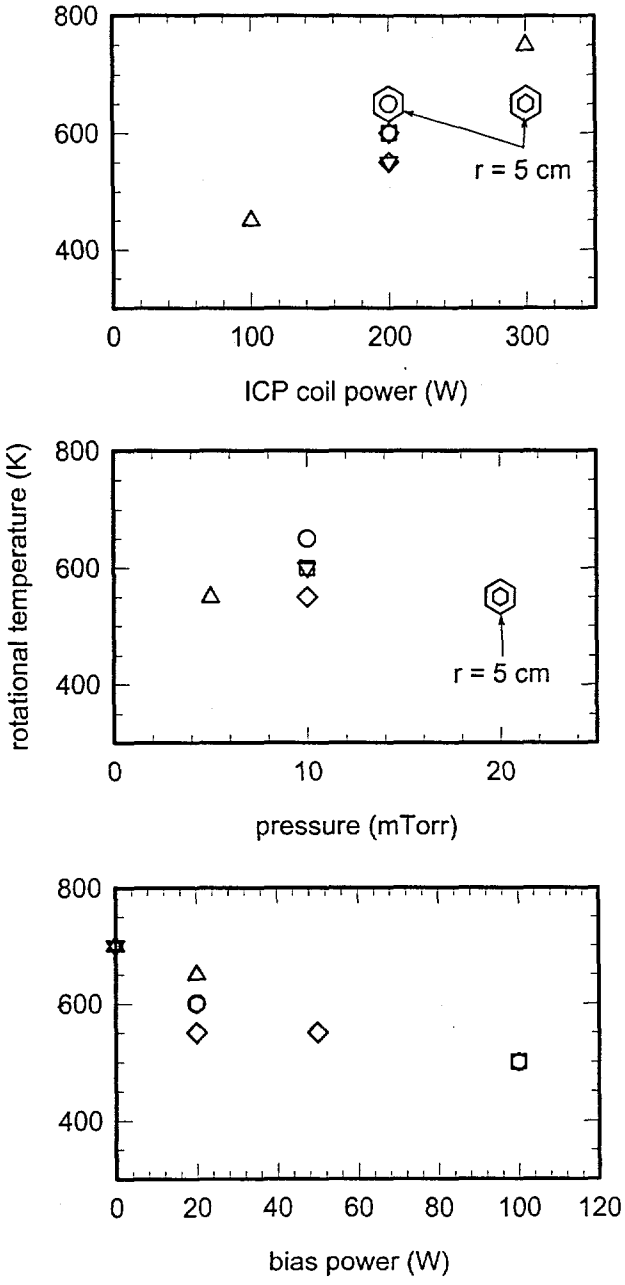
800
600
400
0
100
200
300
r = 5 cm
ICP coil power (W)
rotational temperature (K)
800
600
400
0
10
20
r = 5 cm
pressure (mTorr)
800
600
400
0
20
40
60
80
100
120
bias power (W)

Hebner
Fig 4

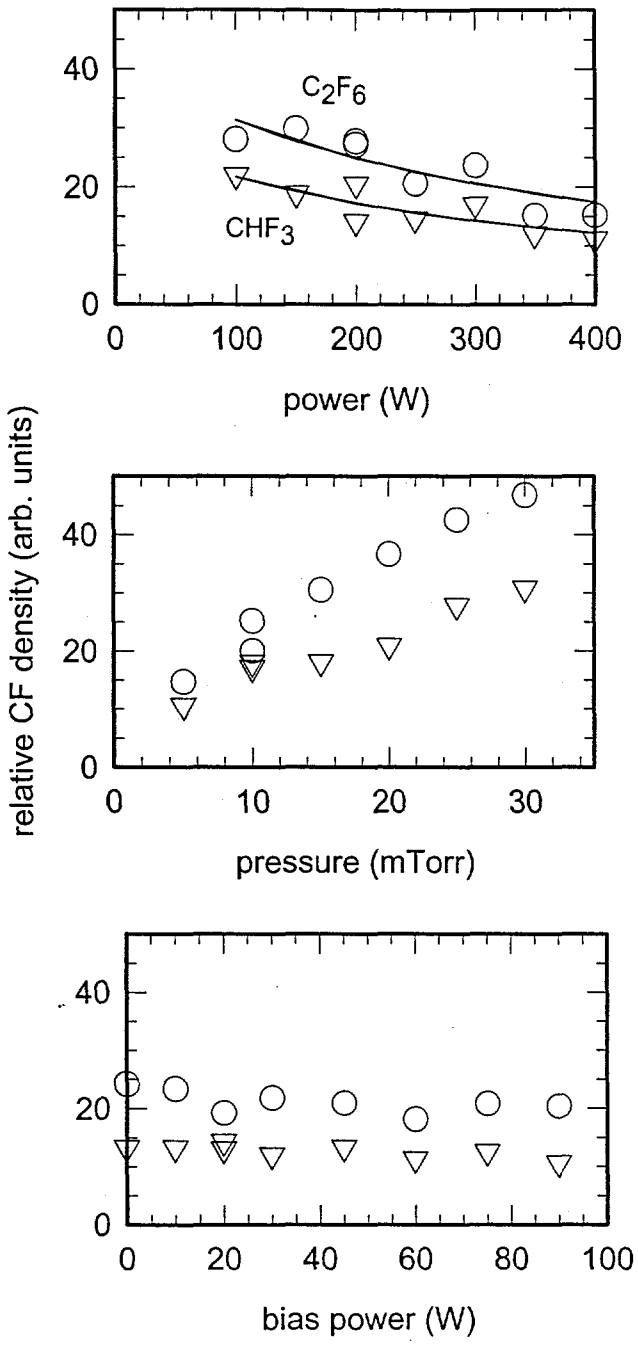
40
20
0
C_2F_6
CHF_3
0
100
200
300
400
power (W)
relative CF density (arb. units)
40
20
0
0
10
20
30
pressure (mTorr)
40
20
0
0
20
40
60
80
100
bias power (W)

Hebner
Fig. 5

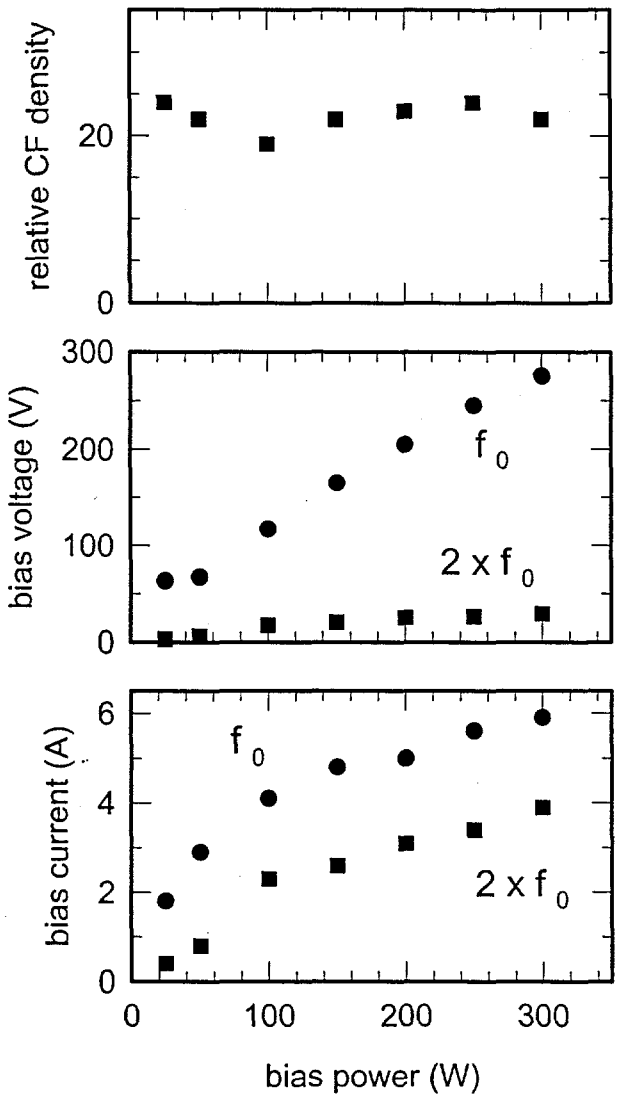
relative CF density
0
20
bias voltage (V)
0
100
200
300
f 0
2 x f 0
bias current (A)
0
2
4
6
f 0
2 x f 0
0
100
200
300
bias power (W)

Hebner
Fig. 6

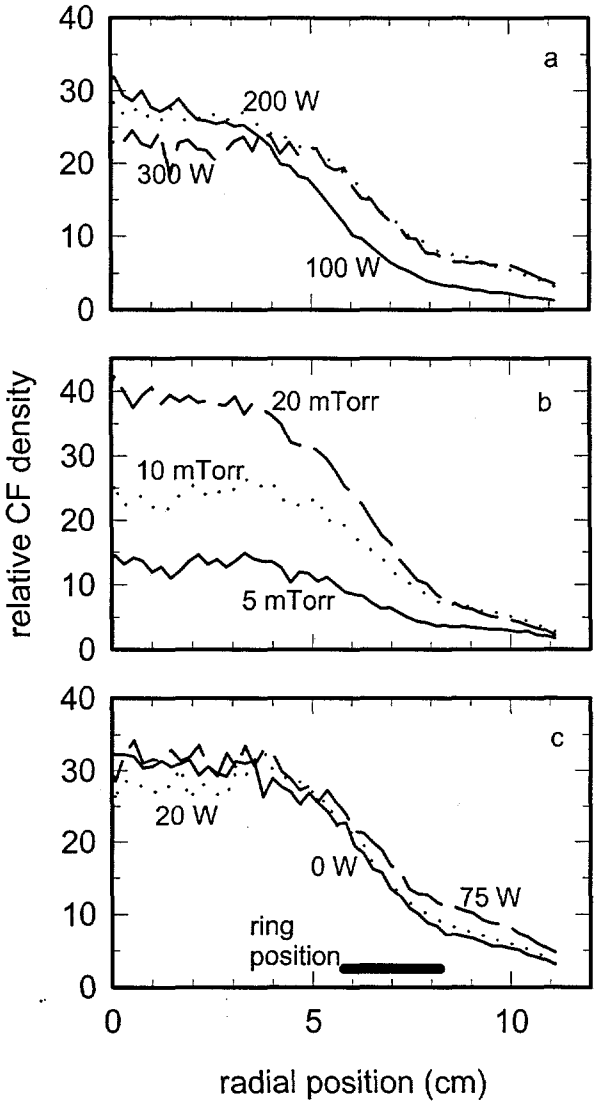
a
200 W
300 W
100 W
b
20 mTorr
10 mTorr
5 mTorr
c
20 W
0 W
75 W
ring
position
relative CF density
radial position (cm)
0
5
10
20
30
40

Hebner
Fig. 7

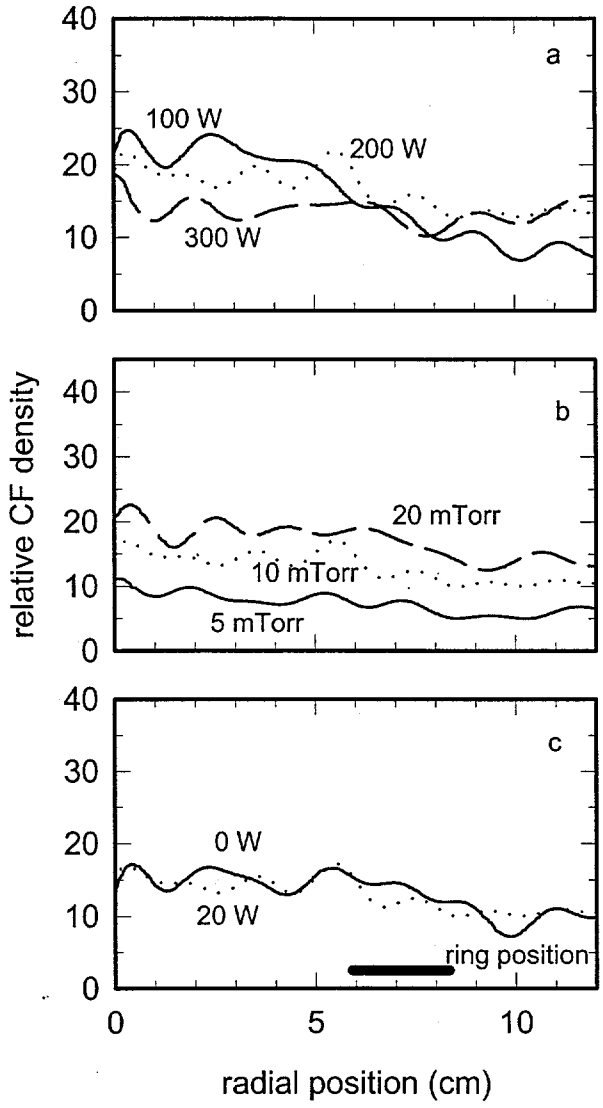
a
100 W
200 W
300 W
b
20 mTorr
10 mTorr
5 mTorr
c
0 W
20 W
ring position
relative CF density
radial position (cm)
0
5
10
0
10
20
30
40

Hebner
Fig. 8

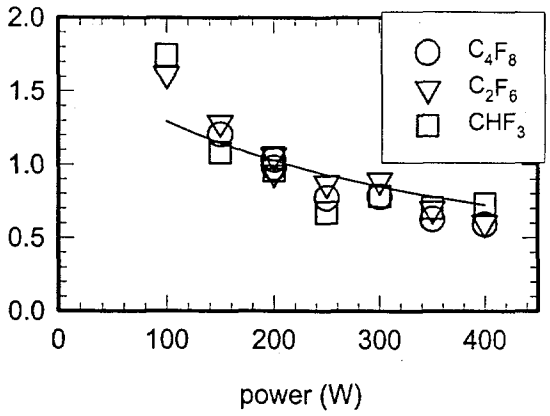
2.0
1.5
1.0
0.5
0.0
0
100
200
300
400
power (W)
C_4F_8
C_2F_6
CHF_3

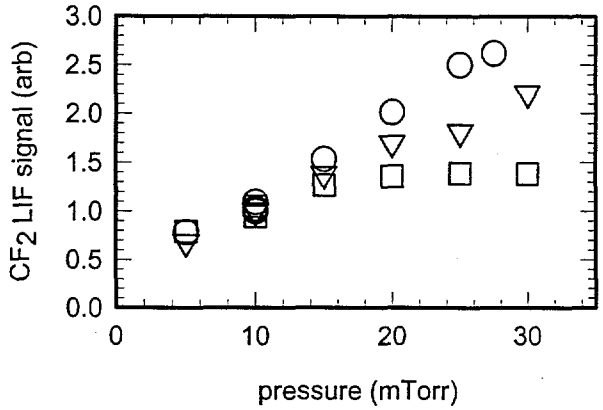
3.0
2.5
2.0
1.5
1.0
0.5
0.0
0
10
20
30
pressure (mTorr)
CF_2 LIF signal (arb)

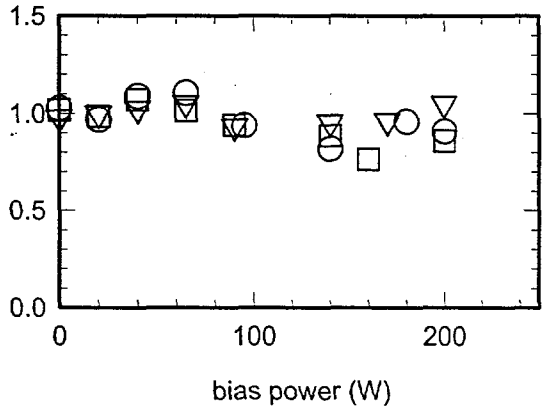
1.5
1.0
0.5
0.0
0
100
200
bias power (W)

Hebner
Fig 9

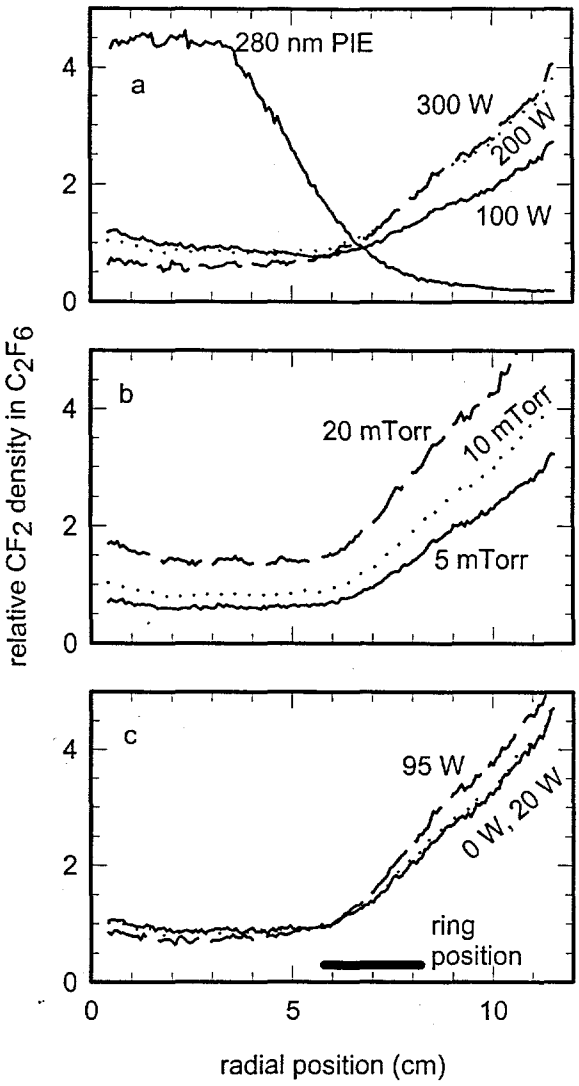

Hebner
Fig. 10

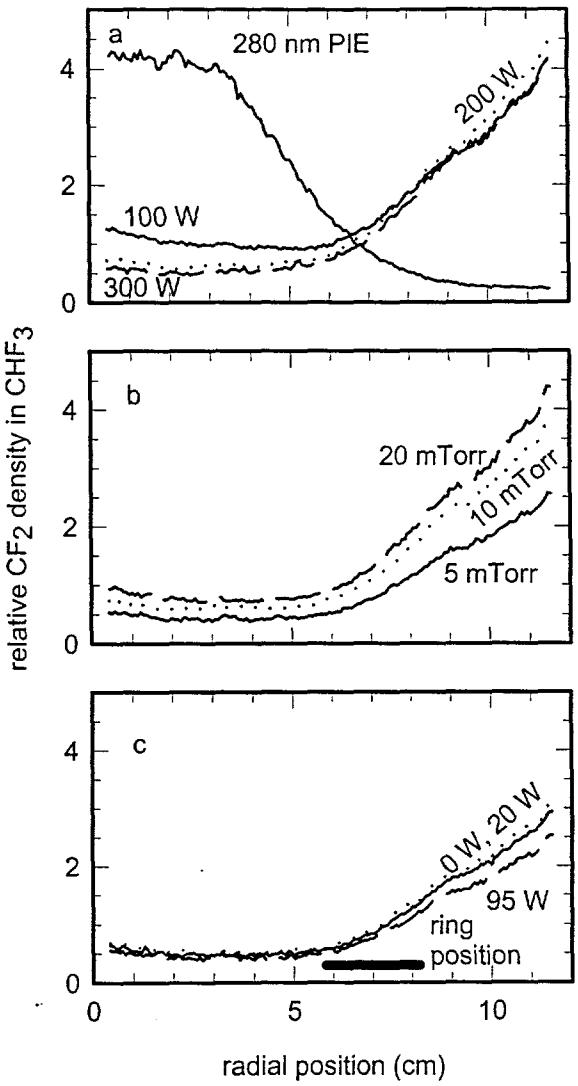

Hebner
Fig. 11

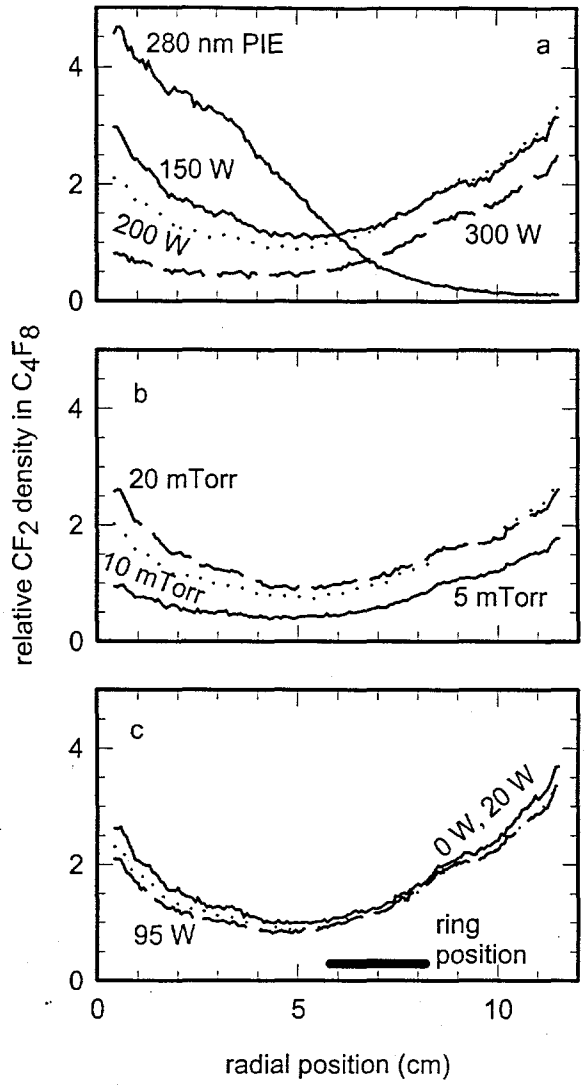

Hebner
Fig. 12

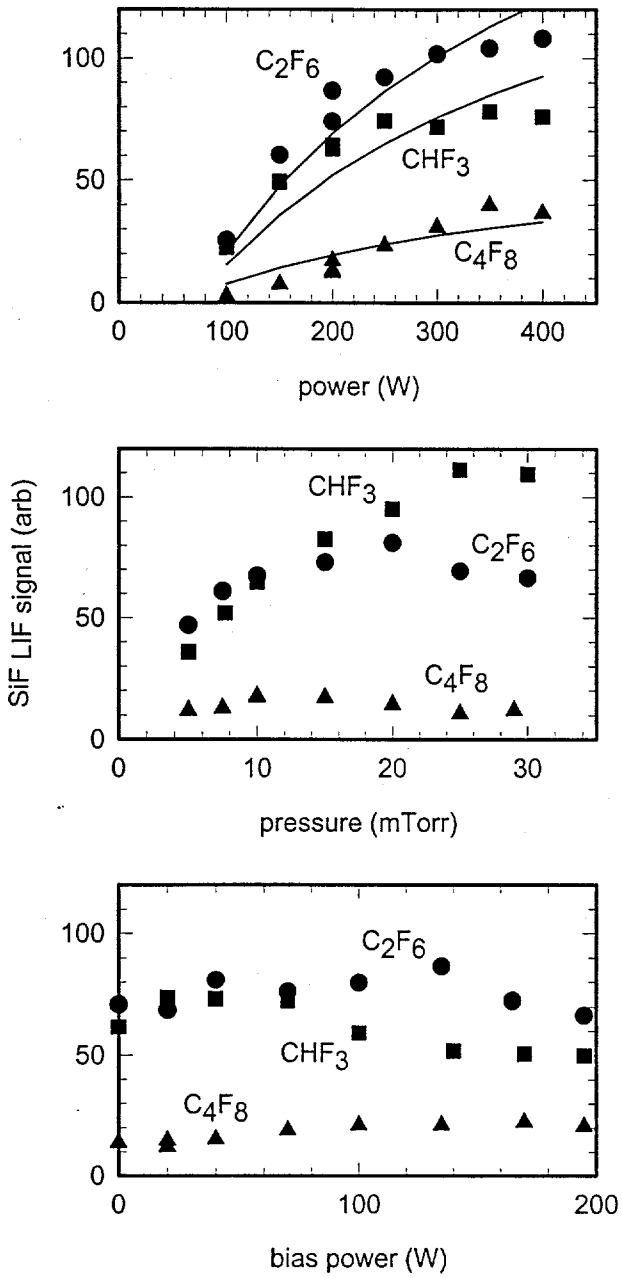

Hebner
Fig. 13